7-14-2011

Artificial lateral line canal for hydrodynamic detection

Yingchen Yang
The University of Texas Rio Grande Valley, yingchen.yang@utrgv.edu

Adrian Klein

Horst Bleckmann

Recommended Citation

Yang, Yingchen, et al. "Artificial lateral line canal for hydrodynamic detection." Applied Physics Letters 99.2 (2011): 023701. https://doi.org/10.1063/1.3610470

Artificial lateral line canal for hydrodynamic detection

Cite as: Appl. Phys. Lett. **99**, 023701 (2011); https://doi.org/10.1063/1.3610470
Submitted: 14 September 2010 • Accepted: 22 June 2011 • Published Online: 14 July 2011

Yingchen Yang, Adrian Klein, Horst Bleckmann, et al.

Artificial lateral line canal for hydrodynamic detection

Yingchen Yang,[1,2] Adrian Klein,[3] Horst Bleckmann,[3] and Chang Liu[1,a)]
[1]*Department of Mechanical Engineering, Northwestern University, Evanston, IIllinois 60208, USA*
[2]*Department of Engineering, University of Texas at Brownsville, Brownsville, Texas 78520, USA*
[3]*Institut für Zoologie, Universität Bonn, Poppelsdorfer Schloss, D-53115 Bonn, Germany*

(Received 14 September 2010; accepted 22 June 2011; published online 14 July 2011)

Fish use their lateral line system to detect minute water motions. The lateral line consists of superficial neuromasts and canal neuromasts. The response properties of canal neuromasts differ from those of superficial ones. Here, we report the design, fabrication, and characterization of an artificial lateral line canal system. The characterization was done under various fluid conditions, including dipolar excitation and turbulent flow. The experimental results with dipole excitation match well with a mathematical model. Canal sensors also demonstrate significantly better noise immunity compared with superficial ones. Canal-type artificial lateral lines may become important for underwater flow sensing. © *2011 American Institute of Physics*. [doi:10.1063/1.3610470]

Fish use the mechanosensory lateral line to detect nearby weak water motions and pressure gradients. Lateral line information enables fish to avoid predators, track prey, swim in schools, maintain position in turbulent environments, and circumnavigate underwater objects.[1–4] The basic unit of the lateral line is the neuromast, a mechanosensitive structure that consists of hair cells whose ciliary bundles project into a gelatinous cupula.[5] Up to several thousand, neuromasts, distributed across the head, body, and tail fin of fish, constitute the lateral line system. Lateral line neuromasts fall into two categories: superficial neuromasts that are located on the skin and canal neuromasts that are situated in subepidermal fluid-filled canals.[5,6] Canal neuromasts respond to the outside flow through a series of pores opening to the environment. Local pressure gradients outside the fish induce fluid movement inside lateral line canals that in turn displace the cupulae of canal neuromasts and elicit a neuronal response in the afferent nerve fibers that innervate the neuromast.[7]

Canal neuromasts have some unique response properties not observed in superficial neuromasts.[8–11] One is a band-pass filtering feature. Canal neuromasts are insensitive to the DC-component of bulk water flow velocity and to high-frequency (>100 Hz for the ruffe)[8] flow velocity fluctuations. The selective sensing of mid-frequencies may be crucial for the survival of fish: Hydrodynamic disturbances caused by other animals are mainly in the frequency range of 0.5 to about 100 Hz.[10] The second characteristic is the noise rejection. The lateral line canal system rejects most of the background noise caused by bulk water flow.[11] This leads to an increase in the signal-to-noise ratio and thus eases the detection of prey-borne stimuli.[8] Further, lateral line canals provide a physical protection to the canal neuromasts.[12]

A man-made artificial lateral line system may be important for many engineering applications, especially for underwater robots and vehicles. In our earlier research, artificial lateral lines based on superficial neuromasts have been demonstrated.[13,14] In the present work, we developed an artificial lateral line canal (ALLC) and characterized its response properties. Both band-pass filtering and noise-rejection functions were examined.

Biomimetic neuromasts (BNs, Fig. 1(a)) developed in our earlier work[15] were employed to constitute the ALLC. The BN characterization in water flow shows a standard deviation of less than 5% of the mean flow velocity employed.[15] In ALLC fabrication, the BN array was flush-mounted in a milled slot on a printed circuit board (PCB), with the sensing directions of individual BNs all along the array (Fig. 1(b)). The canal structure was fabricated using stereolithography technique. It was then assembled to the BN array and held down by glue. The BNs were wire-bonded to the PCB to achieve electrical connection to the outside circuit. After encapsulating the wire-bonds with epoxy glue, the yielded ALLC structure was planarized using polydimethylsiloxane (PDMS) to form a smooth front surface (Fig. 1(c)). The canal (diameter 4 mm) had a semicylindrical shape. The pores (diameter 0.8 mm) were evenly distributed with a spacing of 6 mm, i.e., with a spacing that matched the BN spacing.

A physical-mathematical model was developed to characterize the ALLC before testing. The model was adapted from an analytical study on arthropod filiform hairs by

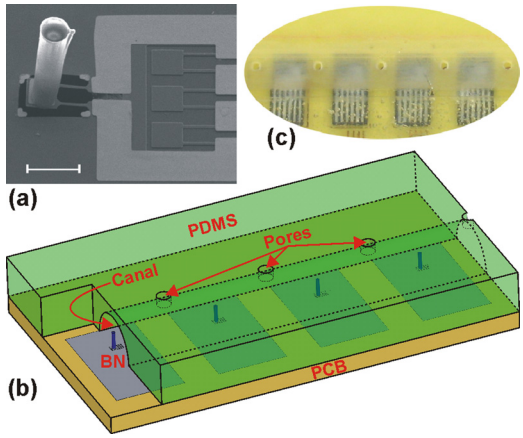

FIG. 1. (a) (Color online) Scanning electron micrograph of a BN. (b) Diagram illustrating the structural detail of the ALLC. (c) Picture of the assembled ALLC.

a)Author to whom correspondence should be addressed. Electronic mail: changliu@northwestern.edu.

Humphrey *et al.*,[16] with notable variations being incorporated. Our BNs more closely resembled the morphological structure of filiform hairs rather than the structure of fish neuromasts that have a nearly hemispherical shape.[9] This is attributed to the current microfabrication process.

The BN's hair (550 μm tall, 80 μm in diameter) is modeled as a rigid body with no deformation under load, but the silicon cantilever beam where the hair sits is much more deformable. Thus, the flow-induced free-end angular deflection of the beam is the same as the rigid hair's angular displacement. Under periodic oscillating boundary layer conditions, the governing equation of the BN hair's angular displacement θ is the conservation of angular momentum

$$(I + I_\rho + I_\mu)\ddot{\theta} + R_\mu\dot{\theta} + S\theta = 4\pi\mu G\int_0^H V_F y dy + \left(\frac{\pi\rho d^2}{4} - \frac{\pi\mu G}{2fg}\right)\int_0^H \dot{V}_F y dy, \quad (1)$$

where ρ, μ, f, d, H, I, I_ρ, I_μ, R_μ, S, G, and g are parameter as defined in Humphrey *et al.*[16] V_F is the velocity profile inside the canal caused by the oscillatory pressure gradient between the two adjacent pores. In the modeling, the semicircular cross-section of the canal in the ALLC was approximated as a circular cross-section with the same hydraulic diameter, which is 2.4 mm. Then inside the canal of radius $R = 1.2$ mm, at a distance r from the canal axis, the velocity of an oscillating flow driven by pressure gradient can be described as

$$V_F(r,f,t) = A_0 e^{i2\pi ft}\frac{-i}{2\pi f}\left[1 - \frac{J_0\left(\sqrt{-2i}\frac{r}{\delta}\right)}{J_0\left(\sqrt{-2i}\frac{R}{\delta}\right)}\right], \quad (2)$$

where J_0, δ, and A_0 are defined in van Netten.[8]

Using a numerical approach, the velocity profile V_F and its time derivative $\dot{V}_F$ can be calculated from Eq. (2), and the two integrals over the height H of the hair in Eq. (1) can be obtained. Based on that, numerically solving Eq. (1) gives the angular displacement θ of the hair under specified conditions. Using this physical-mathematical model, the steady-state angular displacement of the hair in response to the frequency variation of the oscillatory canal flow under a fixed acceleration amplitude of the external water flow was generated and plotted in Fig. 2. For convenience purpose, the acceleration amplitude was chosen to be 1 m/s^2 that corresponded to a pressure gradient amplitude along the canal of 1 KPa/m. For the ALLC with dimensions and geometric approximation specified in the foregoing, the numerical results suggest a band-pass characteristic with a peak at 0.4 Hz. Below the peak frequency, BN response decreases mildly with decreasing frequency. Yet, remarkable drop can still be observed when the frequency is approaching zero. Above the peak frequency, it drops at a much steeper slope with increasing frequency. This frequency response trend of the ALLC resembles that of a canal neuromast in fish, as illustrated in Fig. 7 by van Netten.[8] Depending on the fish species, the peak frequencies of canal neuromasts may vary from below 1 Hz to a few hundred Hertz.[8] In comparison, the demonstrated ALLC emulates a lower end case of its biological counterpart, representing a big fish.

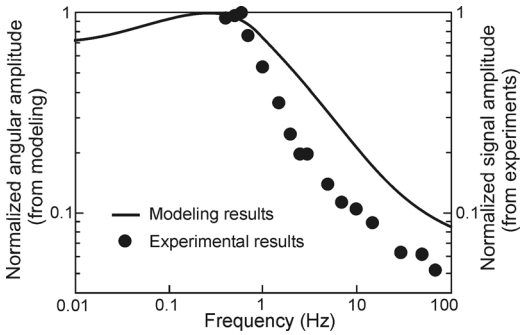

FIG. 2. Frequency responses of the BN in terms of the hair's angular displacement from modeling and the sensor output from experiments, normalized with their maxima.

The ALLC's modeling results were also verified experimentally in a dipolar flow field. A sphere (radius $a = 6.4$ mm), attached to a minishaker, was vertically vibrated in water to serve as a dipole source. The ALLC was placed in water horizontally with all the pores facing up. The dipole source was right above one pore (namely P1), and the distance from the center of the dipole source to the top surface of the ALLC is $l = 11.4$ mm. Using a dipole analytical model,[17] the pressure gradient between the pore P1 and the adjacent pore P2, with a spacing of $\Delta x = 6$ mm, can be expressed as

$$\frac{dp}{dx} = \left(\frac{1}{l^2} - \frac{l}{(l^2 + (\Delta x)^2)^{3/2}}\right)\frac{\rho a^3}{2\Delta x}A_s \sin(2\pi ft), \quad (3)$$

where A_s is the acceleration amplitude of the sphere. During the experiments, the dipole frequency f was swept from 0.4 Hz up to 95 Hz. For comparison with modeling results, the pressure gradient was maintained constant at $dp/dx = 1$ KPa/m. This was achieved by monitoring the dipole acceleration using an accelerometer attached to the minishaker. The pressure gradient amplitude was then calculated using Eq. (3) based on the reading from the accelerometer.

The experimental results are also plotted in Fig. 2 in terms of BN output versus sphere vibration frequency. Note that for our BN with the structure as illustrated in Fig. 1(a), its output is linearly proportional to the hair's angular displacement.[15] Therefore, after normalization with maxima, the experimental results are directly comparable with the modeling results. Overall, the results from the two approaches match reasonably well—they both show a mild climbing followed by a quick drop. The peak frequency from experiments is 0.6 Hz, which is a little higher than the 0.4 Hz obtained from modeling. The small discrepancy is mainly due to the geometrical approximation of the canal from a semicircular cross-section in experiments to a circular cross-section in the modeling, both having the same hydraulic diameter. It should be noted that after the peak, the experimental data fall off faster than the modeling data. Before the peak, the experimental data for very low frequencies were not obtained due to the limited capability of the shaker employed.

Having the band-pass filter function of the ALLC been demonstrated (with near-zero-Hertz response not experimentally examined), the noise-rejection capability was then examined experimentally in the follows. The noise herein is

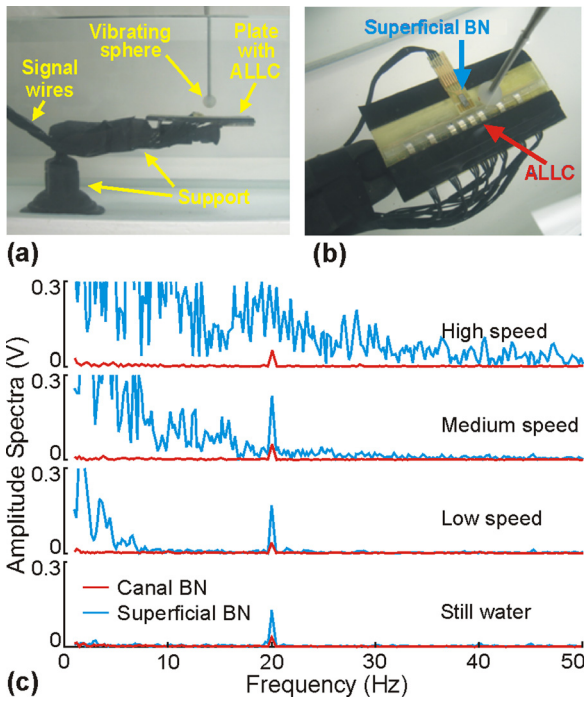

FIG. 3. (Color online) (a) Side view of the experimental setup. The water flow is from right to left, and the sphere shakes up and down. (b) Picture showing the arrangement of the superficial BN, ALLC, and the vibrating sphere. (c) Spectra of the two types of BNs at various inflow velocities. The blue ones are from the superficial BN, and the red ones are from the canal BN.

defined as any random and irregular hydrodynamic signatures that demonstrate broadband spectra with no dominant frequencies. In the present approach, the noise was generated by turbulent flows. Both a canal BN (from the ALLC) and a superficial BN were employed for comparative experiments in a water channel (Fig. 3). A dipole field was superimposed on the channel flow; it was generated by a sphere vibrating at 20 Hz. Note that, this frequency is somewhat away from the ALLC's peak frequency (below 1 Hz). This frequency was chosen in order to obtain a reasonably strong dipolar velocity field, which would otherwise not be able to achieve due to the limited capability of the shaker employed. During the experiments, the two types of BNs were placed close to each other as shown in Fig. 3(b). The turbulent boundary layer flow that developed along the top surface of the plate induced strong hydrodynamic noise to the superficial BNs, and the noise level increased with increasing inflow velocity. Four inflow velocities in the presence of the dipole field were examined: no-flow, low-speed (0.04 m/s), medium-speed (0.08 m/s), and high-speed (0.12 m/s).

Fig. 3(c) shows the spectra of the output signals of the two BNs. Each spectrum was directly derived from a single-set raw data without filtering. In still water with a dipole field only, both the superficial BN and canal BN clearly show peaks at the dipole frequency. The signal from the superficial BN is much stronger than that from the canal BN for two main reasons: (i) the superficial BN was closer to the dipole source than the canal BN (Fig. 3(b)), and (ii) the in-canal flow oscillation at the dipole frequency of 20 Hz was attenuated (Fig. 2). As the inflow velocity increases, the signal from the superficial BN becomes increasingly noisy, especially in the low frequency regime. On the other hand, the canal BN is barely affected by the background turbulent noise in the entire observed frequency range. Eventually, the superficial BN becomes overwhelmed by the low frequency noise and renders incapable of detecting the 20 Hz stimulus while the canal BN performs just as well.

The noise-rejection capability of the ALLC is in line with that of a fish canal neuromast.[11] Yet, no matter whether in a fish lateral line canal or in our ALLC, it seems that the noise-rejection capability that filters out background noise in the entire observed frequency range contradicts with the band-pass filter function. While an in-depth understanding of this seemingly contradiction deserves systematic research, we propose a preliminary explanation. The flow outside a canal influences the flow inside the canal via pores, or more specifically, via the pressure difference between the pores. For an oscillatory flow (with the frequency in the range for band-pass) to be fully developed inside the canal, the pressure difference to drive the flow needs to periodically repeat for at least a few cycles. The excited flow is weak in the first cycle and then gradually strengthens and reaches steady oscillatory state in the following cycles. A well-developed and well-organized external flow, e.g., a dipolar flow, can fully excite an oscillatory flow inside the canal in this fashion. In contrast, the turbulent background noise reflects the chaotic nature of the external driving flow that varies quickly and randomly. Consequently, using an external turbulent flow to drive the fluid inside the canal with no successive excitation cycles for nearly any frequency components, it would be hard for any internal flow to fully develop and instantly follow. As a result, the canal possesses a noise-rejection feature.

This work was supported by the DARPA BioSenSE program (Contract No. FA9550-05-1-0459).

[1]J. H. S. Blaxter and L. A. Fuiman, in *The Mechanosensory Lateral Line: Neurobiology and Evolution*, edited by S. Coombs, P. Görner, and H. Münz (Springer, New York, 1989), pp. 481–499.
[2]D. Hoekstra and J. Janssen, Environ. Biol. Fishes **12**, 111 (2006).
[3]B. L. Partridge and T. J. Pitcher, J. Comp. Physiol., A **135**, 315 (1980).
[4]E. S. Hassan, in *The Mechanosensory Lateral Line: Neurobiology and Evolution*, edited by S. Coombs, P. Görner, and H. Münz (Springer, New York, 1989), pp. 217–228.
[5]S. Coombs, J. Janssen, and J. F. Webb, in *Sensory Biology of Aquatic Animals*, edited by J. Atema, R. R. Fay, A. N. Popper, and W. N. Tavolga (Springer, New York, 1988), pp. 553–593.
[6]A. Schmitz, H. Bleckmann, and J. Mogdans, J. Morphol. **269**, 751 (2008).
[7]A. J. Hudspeth, Y. Choe, A. D. Mehta, and P. Martin, Proc. Natl. Acad. Sci. U.S.A. **97**, 11765 (2000).
[8]S. M. van Netten, Biol. Cybern. **94**, 67 (2006).
[9]J. Engelmann, W. Hanke, and H. Bleckmann, Nature **408**, 51 (2000).
[10]H. Bleckmann, *Reception of Hydrodynamic Stimuli in Aquatic and Semiaquatic Animals* (Springer, New York, 1994).
[11]J. Engelmann, W. Hanke, and H. Bleckmann, J. Comp. Physiol., A **188**, 513 (2002).
[12]S. Dijkgraaf, Biol. Rev. **38**, 51 (1962).
[13]Y. Yang, J. Chen, J. Engel, S. Pandya, N. Chen, C. Tucker, S. Coombs, D. L. Jones, and C. Liu, Proc. Natl. Acad. Sci. U.S.A. **103**, 18891 (2006).
[14]Y. Yang, N. Nguyen, N. Chen, M. Lockwood, C. Tucker, H. Hu, H. Bleckmann, C. Liu, and D. L. Jones, Bioinspiration Biomimetics **5**, 9 (2010).
[15]N. Chen, C. Tucker, J. Engel, Y. Yang, S. Pandya, and C. Liu, J. Microelectromech. Syst. **16**, 999 (2007).
[16]J. Humphrey, R. Devarakonda, I. Iglesias, and F. G. Barth, Philos. Trans. R. Soc. London, Ser. B **340**, 423 (1993).
[17]A. J. Kalmijn, in *Sensory Biology of Aquatic Animals*, edited by J. Atema, R. R. Fay, A. N. Popper, and W. N. Tavolga (Springer, New York, 1988), pp. 83–130.